Two-dimensional observations of overshielding during a magnetic storm by the Super Dual Auroral Radar Network (SuperDARN) Hokkaido radar

Y. Ebihara,[1] N. Nishitani,[2] T. Kikuchi,[2] T. Ogawa,[3] K. Hosokawa,[4] and M.-C. Fok[5]

Received 13 July 2007; revised 28 September 2007; accepted 6 October 2007; published 25 January 2008.

[1] Two-dimensional observations of ionospheric plasma flows possibly caused by overshielding are reported for the first time. The observations were made by the midlatitude Super Dual Auroral Radar Network Hokkaido radar in Japan during a major magnetic storm on 15 December 2006. The magnetosphere was exposed continuously to a southward interplanetary magnetic field (IMF) for several hours during the main phase of the storm. Immediately following the subsequent northward turning of the IMF, an antisunward plasma flow was observed for about 14 min in the predusk sector at magnetic latitudes of 50°–60°, reaching a maximum line-of-sight speed of 70–80 m/s. These features are consistent with a simulation of coupling between the ring current and the ionosphere associated with an overshielding condition. Within 1 h of the first observation, a similar antisunward flow was observed during a period of southward oriented IMF. However, the simulation cannot account for the antisunward flow in this case. It is suggested that the shielding/overshielding condition is not simply caused by the northward turning of IMF. This second overshielding-like condition is attributable to a sudden contraction of the polar cap associated with the substorm or to a sudden strengthening of the inertial current converted from the abrupt injection of magnetospheric ions. However, neither fully accounts for the observations.

Citation: Ebihara, Y., N. Nishitani, T. Kikuchi, T. Ogawa, K. Hosokawa, and M.-C. Fok (2008), Two-dimensional observations of overshielding during a magnetic storm by the Super Dual Auroral Radar Network (SuperDARN) Hokkaido radar, *J. Geophys. Res.*, *113*, A01213, doi:10.1029/2007JA012641.

1. Introduction

[2] The large-scale convection electric field, driven by interaction between the solar wind and the magnetosphere, is known to be penetrated from high to low latitudes [e.g., *Nishida et al.*, 1966; *Fejer et al.*, 1979, 1990; *Gonzales et al.*, 1979; *Kelley et al.*, 1979; *Kikuchi et al.*, 2000a]. The convection electric field is shielded by the region 2 field-aligned currents. The most plausible generator of the region 2 field-aligned current is thought to be the inhomogeneous distribution of the plasma pressure in the inner magnetosphere, or in the ring current region. More precisely, the field-aligned current can be generated by the misalignment between the plasma pressure gradient and the magnetic field gradient under a simplified condition that the plasma pressure is isotropic. [e.g., *Vasyliunas*, 1970; *Wolf*, 1970; *Jaggi and Wolf*, 1973; *Southwood*, 1977; *Senior and Blanc*, 1984; *Spiro et al.*, 1988; *Peymirat et al.*, 2000; *Toffoletto et al.*, 2003]. The field-aligned currents couple to the conducting ionosphere, leading to the generally dusk-to-dawn electric field. This is called the shielding electric field because the direction of the resultant electric field is opposite to that of the dawn-to-dusk convection electric field. The magnitude of the shielding effect depends on the plasma pressure in the inner magnetosphere [e.g., *Vasyliunas*, 1970; *Wolf*, 1970] and the ionospheric conductivity as well [*Spiro and Wolf*, 1984; *Ebihara et al.*, 2004].

[3] Overshielding occurs when the shielding electric field becomes dominant over the convection electric field. Such a situation emerges when the interplanetary magnetic field (IMF) suddenly turns northward after a prolonged southward orientation because the magnitude of the pressure gradients in the inner magnetosphere remains strong for a while after the sudden decrease in the convection electric field [*Spiro et al.*, 1988; *Peymirat et al.*, 2000]. Overshielding has been suggested in many studies on the basis of one-dimensional radar and geomagnetic observations [e.g., *Fejer et al.*, 1979, 1990; *Gonzales et al.*, 1979; *Kelley et al.*, 1979; *Spiro et al.*, 1988; *Kikuchi et al.*, 2000a, 2000b, 2003; *Chakrabarty et al.*, 2006], and *Goldstein et al.* [2002] showed that overshielding may be responsible for a plasmaspheric shoulder on the basis of IMAGE/EUV imager data.

[1] Institute for Advanced Research, Nagoya University, Nagoya, Japan.
[2] Solar-Terrestrial Environment Laboratory, Nagoya University, Nagoya, Japan.
[3] Solar-Terrestrial Environment Laboratory, Nagoya University, Toyokawa, Japan.
[4] University of Electro-Communications, Tokyo, Japan.
[5] NASA Goddard Space Flight Center, Greenbelt, Maryland, USA.

0148-0227/08/2007JA012641

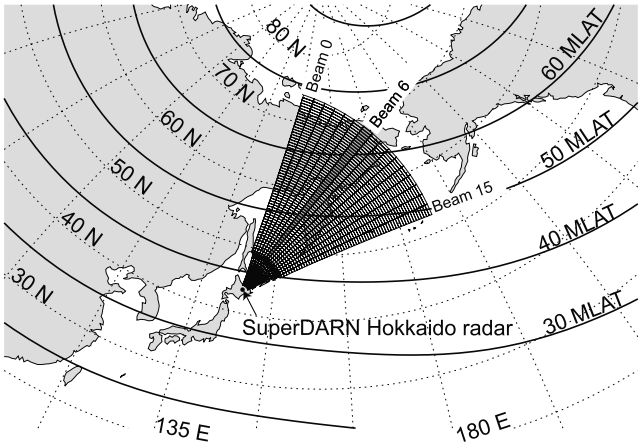

Figure 1. Field of view of the SuperDARN Hokkaido radar. Thick contour lines indicate magnetic latitude at 300 km altitude.

[4] The Super Dual Auroral Radar Network (SuperDARN) is a global network of HF radars capable of measuring backscatter from the ionospheric *E* and *F* regions [*Greenwald et al.*, 1995]. Most of the SuperDARN radars have the field of view covering the high-latitude regions. Recently, a new SuperDARN radar was developed at Rikubetsu in Hokkaido, Japan, which covers a wide area of the subauroral region and is suitable for acquiring the two-dimensional data required for reliable analysis of the shielding/overshielding condition. The great advantage of the two-dimensional observation is to determine the spatial structure of the electric field associated with the shielding/overshielding. The spatial extent and evolution of the electric field distribution is necessary to identify the source of the overshielding electric potential. This paper demonstrates for the first time that the SuperDARN radar is capable in measuring the overshielding electric field and at least one of two overshielding events is attributable to the electric potential that could have been imposed around 60 magnetic latitude (MLAT) by the field-aligned current generated by inhomogeneous distribution of the plasma pressure in the inner magnetosphere.

2. Observation

[5] The SuperDARN Hokkaido radar (43.53°N, 143.61°E) is located at 36.5 MLAT (MLT − UT = 9.3 h), and has a field of view covering magnetic latitudes (MLATs) of 38°–68° as shown in Figure 1. On 15 December 2006, the Hokkaido radar detected brief antisunward flows at subauroral latitudes in the afternoon sector associated with an intense magnetic storm. Figure 2 shows a summary of the solar wind conditions and the provisional

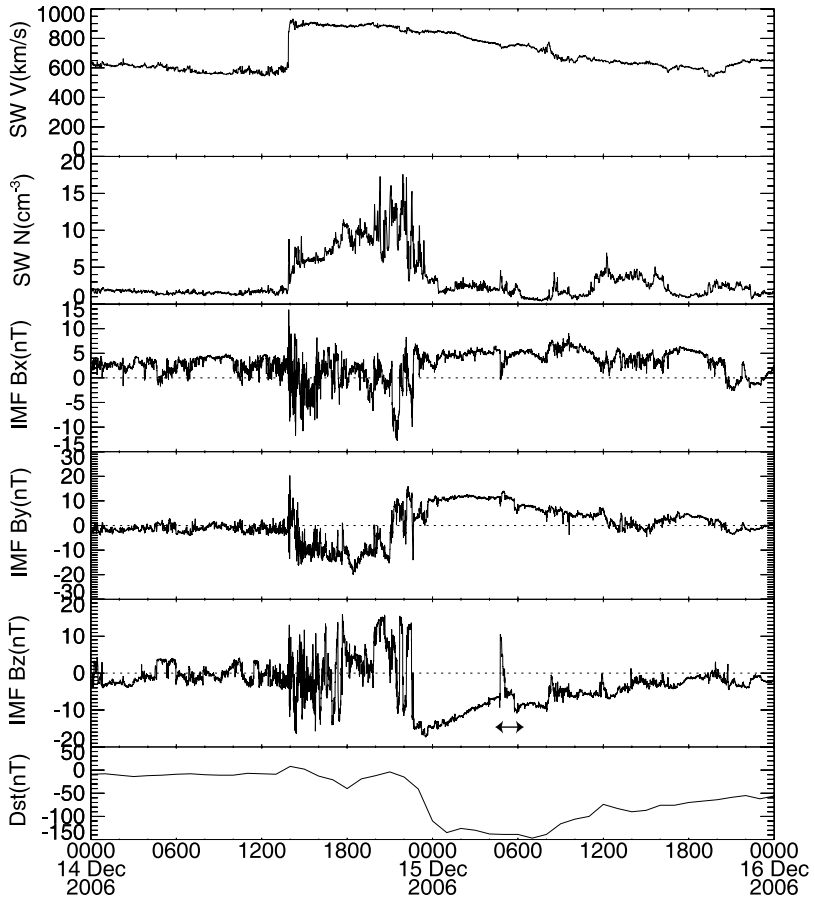

Figure 2. Summary of key parameters of the magnetic storm on 14–15 December 2006. SW V denotes solar wind velocity, and SW N denotes solar wind density. *Dst* index values shown here are provisional values. Solar wind and IMF data were obtained by the ACE satellite.

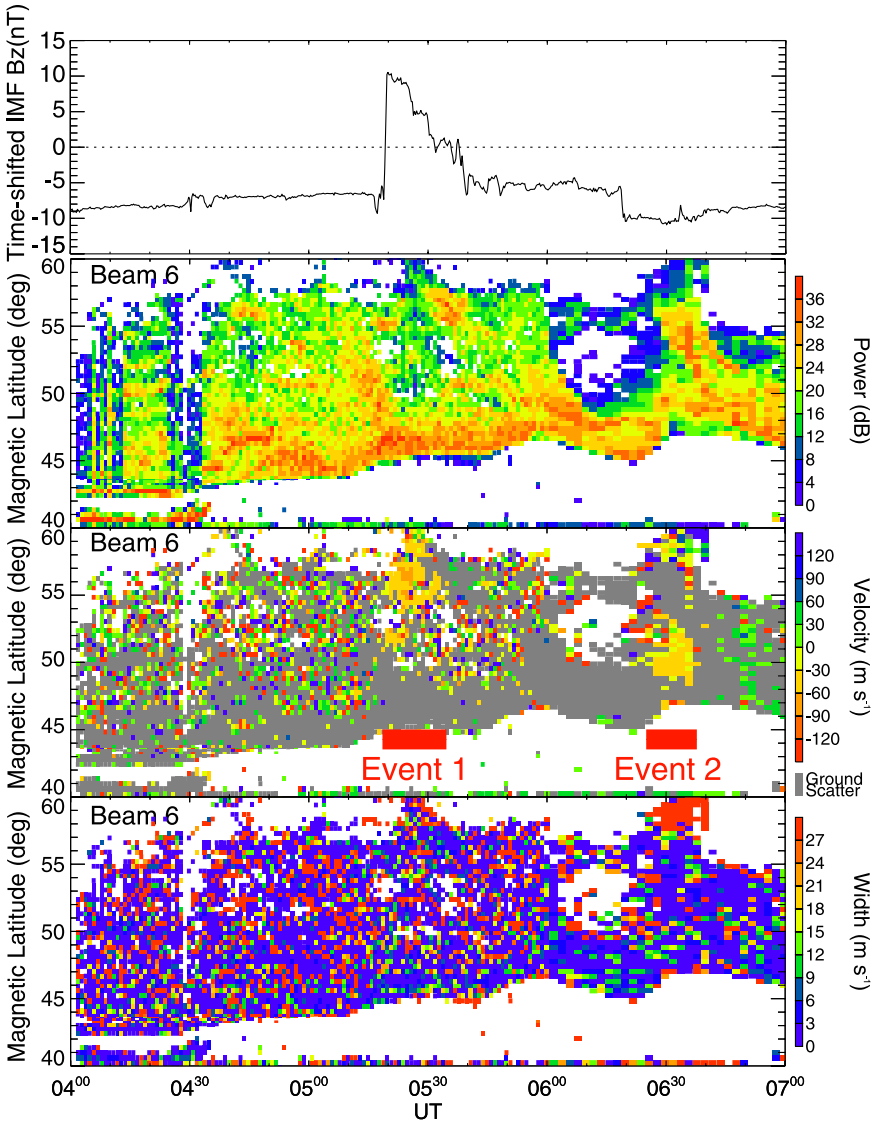

Figure 3. Summary of SuperDARN Hokkaido radar data for 0400–0700 UT, 15 December 15 2006. Time-shifted IMF B_z data were obtained by the ACE satellite. Echo power, line-of-sight Doppler velocity (positive toward the radar), and spectral width along beam 6 are shown as range-time plots. Negative Doppler velocities observed at 0519–0533 UT (event 1) and 0627–0637 UT (event 2) are indicated.

Dst index during the intense magnetic storm of 14–15 December 2006. The storm occurred because of a combination of a prolonged southward IMF and a fast solar wind. The *Dst* index reached −147 nT at 0700 universal time (UT) on 15 December 2006. Approximately 6 h after the IMF turned southward, the IMF turned abruptly northward at 0445 UT. This is the moment at which the overshielding condition is expected to emerge. The solar wind and IMF data were obtained by the Advanced Composition Explorer (ACE) satellite at about 228 R_E upstream of the Earth. The Geotail satellite observed a similar brief northward excursion at about 15 R_E near dawn at 0519 UT (data not shown), providing an accurate estimate of 34 min for propagation of the northward turning from the ACE position to the Earth.

[6] Figure 3 summarizes the Hokkaido radar measurements of backscatter power, Doppler velocity, and spectral width for beam 6. At least two negative velocity regions can be identified. The first (event 1) emerged between 0519 and 0533 UT, extending from 52 to 59 MLAT along beam 6. The maximum speed of approximately 70 m/s occurred near 56–57 MLAT at 0524–0526 UT. The appearance and disappearance of this negative velocity region coincided closely with the northward and southward turnings of the IMF, respectively. The second event (event 2) emerged in the 47–53 MLAT interval at 0627–0637 UT. The magnitude of Doppler velocity for this event exhibits a similar pattern to that of event 1. However, unlike event 1, the IMF B_z remained negative during event 2.

[7] Figure 4 presents snapshots of the line-of-sight velocities in MLAT versus magnetic local time (MLT) coordinates at 1 min intervals during event 1. The negative Doppler velocity region occurs patchily in the subauroral region (46–58 MLAT) in the predusk sector (1500–1800 MLT). The DMSP F13 satellite, which crossed the field of

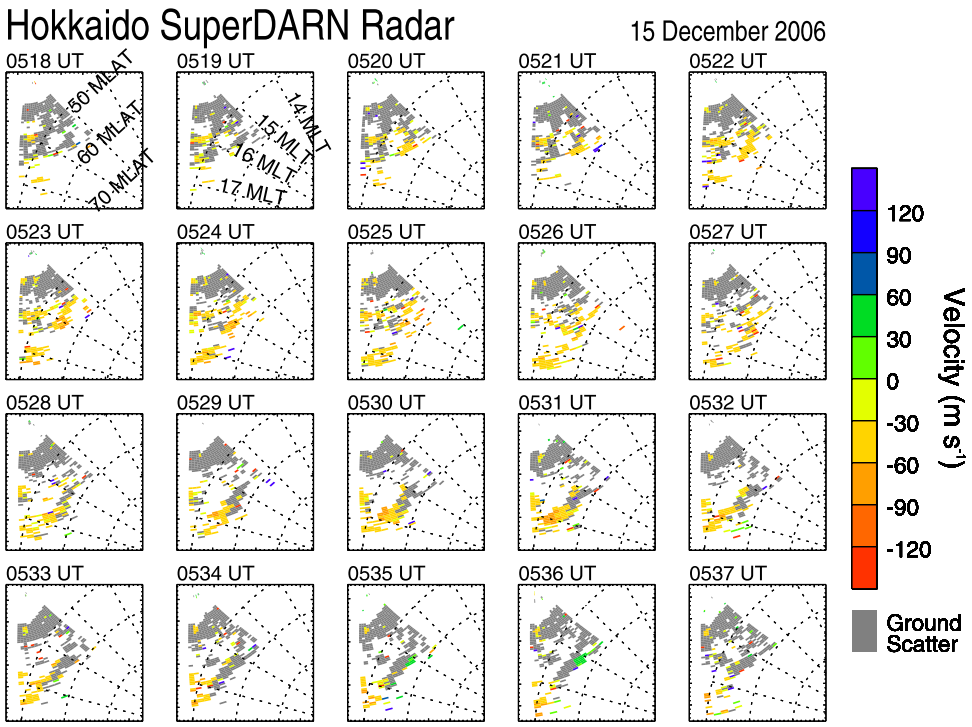

Figure 4. Snapshots of Doppler velocity during event 1 in MLT-MLAT coordinates (Sun at top). Positive Doppler velocity represents flow toward the radar.

view of the Hokkaido radar about 20 min after the onset of event 1, detected the equatorward edge of the electron precipitation at 57 MLAT. This observation indicates that event 1 occurred in the region equatorward of the inner edge of electron precipitation in the plasma sheet. The direction of the brief negative flow is dominated by an antisunward component, opposite to that observed typically in the subauroral region on the eveningside [e.g., *Foster and Vo*, 2002; *Weimer*, 2005; *Ruohoniemi and Greenwald*, 2005].

3. Simulation

[8] A numerical simulation solving the kinetic equation for energetic ions trapped in the inner magnetosphere as well as closure of the electric current between the inner magnetosphere and the ionosphere was conducted using the simulation model described in detail by *Fok et al.* [2001] and *Ebihara et al.* [2004]. The bounce-averaged drift velocities were calculated under the magnetic field determined by the Tsyganenko-1996 empirical model [*Tsyganenko*, 1995; *Tsyganenko and Stern*, 1996] and the electric field determined by the requirement of continuity of electric current in the coupled magnetosphere-ionosphere system. The electric potential given by the *Weimer* [2001] convection electric field model (dependent on the solar wind condition) was imposed as a boundary condition for the simulation (at 66.7 MLAT). The corotation electric field was also included. The height-integrated conductivity in the ionosphere was modeled as due to the conductivity caused by solar illumination and that caused by auroral precipitating electrons. The former was calculated using the International Reference Ionosphere (IRI-95) [*Bilitza*, 1997] and the Mass Spectrometer Incoherent Scatter (MSIS-E90) models [*Hedin*, 1991], and the latter was calculated using an empirical model dependent on *Kp* [*Hardy et al.*, 1987]. The phase space density of ions at the simulation boundary was assumed to be given by the isotropic Maxwellian with a density of 0.75 cm^{-3} and temperature of 5 keV.

[9] Figure 5 shows the temporal variations in perpendicular plasma pressure in the equatorial plane and the field-aligned current at an ionospheric altitude of 100 km at 0514 UT (prior to northward turning), 0520 UT (after northward turning), and 0540 UT (after southward turning). The pressure maximum conspicuously lies in the dusk-midnight sector as a consequence of the drift motion of ions. The axial asymmetry of the pressure distribution generates the azimuthal component of the pressure gradient, resulting in the misalignment between the plasma pressure gradient and the magnetic field gradient. The misalignment is greater in the predusk region and predawn region than in between. Thus there is a tendency that a field-aligned current flows into the ionosphere in the predusk region and a current away from the ionosphere in the predawn region. Prior to the northward turning of the IMF (0514 UT), the electric potential is dominated by the convection electric potential. The focuses of the normal two-cell convection vortices are located inside the poleward boundary of the simulation region where we did not solve the electric potential. The line-of-sight velocity is slightly negative (away from the radar) at MLATs less than about 55° as shown in blue arrows because of influence of the relatively weak shielding effect. At MLATs greater than 55°, the line-of-sight velocity is positive (toward the radar) under the influence of the convection electric field. Immediately after the northward turning of the IMF (0520 UT), the ionospheric plasma flow changed markedly because of the sudden decrease in

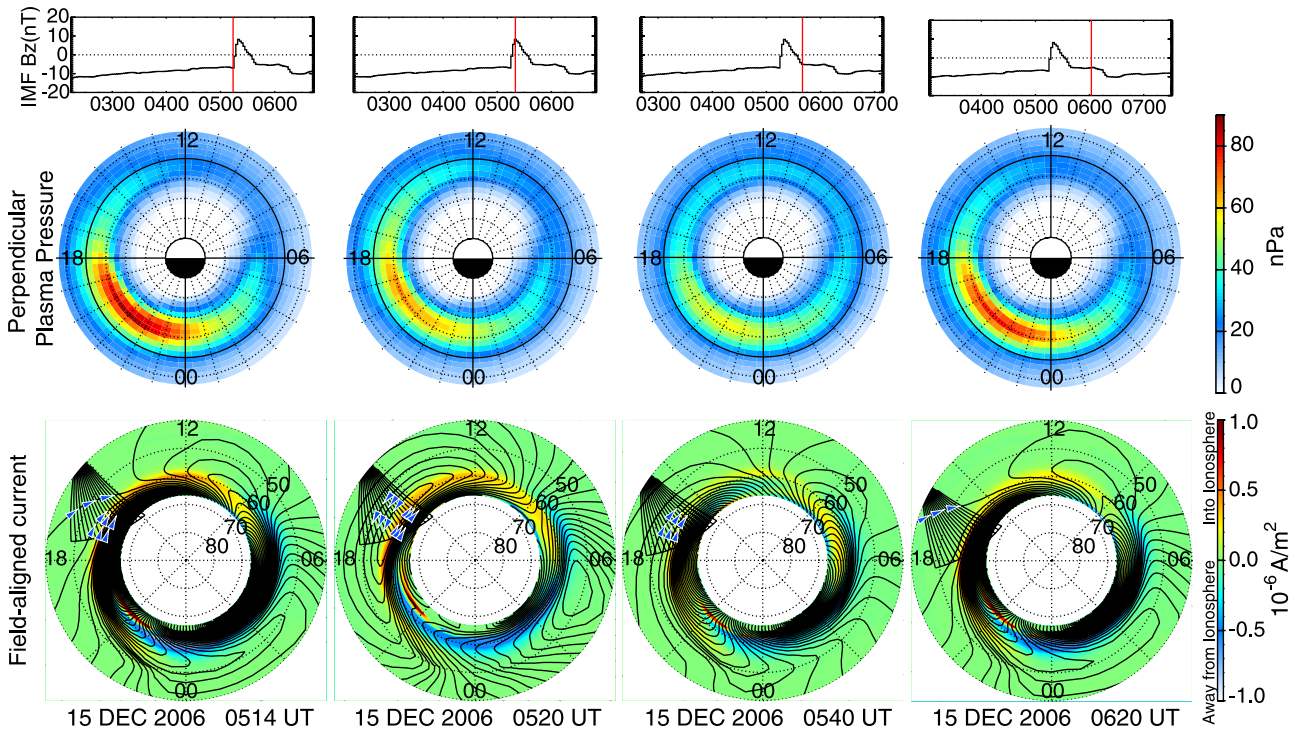

Figure 5. Summary of simulation results. (top) Time-shifted IMF B_z data were used as one of the input parameters of the simulation. (bottom) Circular plots show perpendicular plasma pressure in the equatorial plane and field-aligned current at ionospheric altitude. Calculated electric potential is shown by contours. Arrows indicate the direction of plasma flow in the rotating Earth frame of reference (Sun at top).

convection electric potential. The electric potential generated by the asymmetry of the plasma pressure in the inner magnetosphere appears to become dominant over the convection electric field. Two flow vortices are obvious in the subauroral region, one in the dusk sector (counterclockwise) and one in the dawn sector (clockwise). The radar thus observed plasma flow away from the radar in the equatorward portion of the vortex. After the southward turning of the IMF, the convection electric field again becomes dominant over the electric potential.

[10] Figure 6 shows a simulated range-time plot of the line-of-sight velocity along beam 6 of the Hokkaido radar. A brief negative velocity region was apparent during the period of the northward IMF (0519–0533 UT). The maximum speed of about 50 m/s was reached near 57 MLAT at 0524 UT, approximately 5 min after the northward turning of the IMF. These characteristics are consistent with the characteristics of event 1 detected by the Hokkaido radar. From the close similarity between the simulation and the observations, it is concluded that event 1 is associated

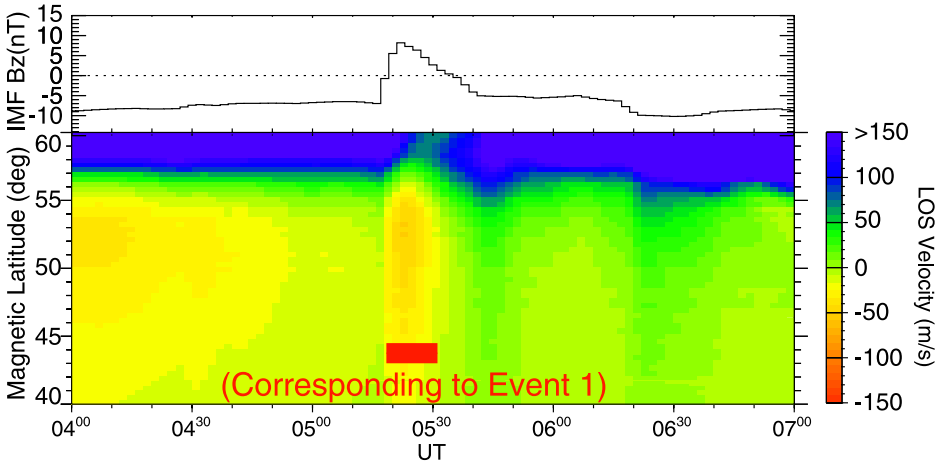

Figure 6. Simulated range-time plot of line-of-sight velocity (positive toward the radar) of ionospheric plasma flow along beam 6 of the SuperDARN Hokkaido radar at 0400–0700 UT, 15 December 2006.

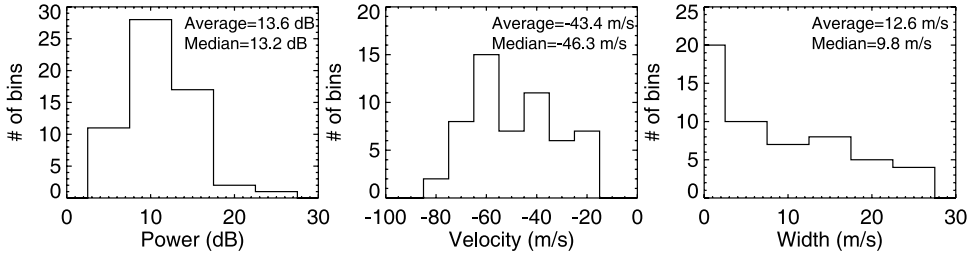

Figure 7. Statistical distributions of echo power, Doppler velocity, and spectral width of echoes in the negative Doppler velocity region (53.4–57.0 MLAT, 15.8–16.3 MLT).

directly with an overshielding condition caused by the sudden northward turning of the IMF. For event 2, no obvious negative velocity region comparable to the radar observations is identifiable in the simulated range-time plot. The difference between the simulation and the observations for event 2 is discussed below.

4. Discussion

[11] Ray tracing using models of the ionosphere and magnetic field [*Nishitani and Ogawa*, 2005] indicates that the patchy Doppler velocity regions correspond to the regions where high-frequency (HF) radar wave vector is orthogonal to the ambient magnetic field. Thus the Doppler velocity appears to correspond to the line-of-sight velocity of the ionospheric plasma. To confirm this, the characteristics of the echoes are shown in Figure 7. Data collection from beams 5, 6, 7 and 8 and range gates from 49 to 53 (MLAT ranging between 53.4° and 57.0°) during the period from 0523 UT to 0528 UT were chosen to illustrate Figure 7. The statistical distributions of echo power, Doppler velocity, and spectral width in the negative Doppler velocity region (53.4–57.0 MLAT, 15.8–16.3 MLT) are characterized by moderately strong backscatter power (mean power, 13.6 dB), relatively slow Doppler velocity (mean velocity, −43.4 m/s), and relatively narrow spectral width (mean width, 12.6 m/s). The echoes are readily distinguished from ground (or sea) scatter echoes as reported by, e.g., *Samson et al.* [1989] and *Bristow and Greenwald* [1997]. They showed that the ground (or sea) scatter echoes associated with medium-scale traveling ionospheric disturbance (MSTID) have Doppler velocity amplitudes less than 18 m/s.

[12] These characteristics are similar to those observed by the SuperDARN Wallops radar in the subauroral and postsunset region [*Greenwald et al.*, 2006]. The solar zenith angle (−99° to −96°) during the observation indicates that the backscatter took place in the postsunset region. By analogy with the Wallops measurements, the backscatter echoes observed by the Hokkaido radar are considered to be due to irregularities produced by temperature gradient instability (TGI) [e.g., *Hudson and Kelley*, 1976; *Greenwald et al.*, 2006]. The TGI is suggested to be generated in the region in which the electron density gradient is directed opposite to the electron temperature gradient [*Hudson and Kelley*, 1976]. The radar echoes may also be associated with the gradient drift instability (GDI) [e.g., *Hosokawa et al.*, 2001]. The plasma is known to be unstable to GDI when the direction of the plasma velocity is the same as the direction of the background plasma density gradient. In addition, upward field-aligned currents are also suggested to cause the *F* region irregularities [*Ossakow and Chaturvedi*, 1979]. However, as there is neither incoherent scatter radar nor auroral imager situated under the field of view of the Hokkaido radar, there is no direct means of identifying the possible source of *F* region irregularities responsible for the backscatter. A reasonable explanation for the ionospheric irregularities is therefore needed in order to confirm theoretically that the echo indeed returned from the ionosphere, and is not due to ground or sea scatter.

[13] Comparison of the simulations and observations indicates that event 1 is most likely attributable to an overshielding condition caused by the sudden northward turning of the IMF. Conventional models of the inferred overshielding mechanism [*Spiro et al.*, 1988; *Fejer et al.*, 1990; *Peymirat et al.*, 2000; *Kikuchi et al.*, 2000a, 2003] suggest that the enhanced convection electric field during the southward IMF sets up a ring current that produced region 2 field-aligned currents. The sudden northward turning of the IMF would then have resulted in a rapid weakening of the convection electric field, while the field-aligned current produced by the ring current, which cannot be weakened quickly, would have persisted for some time. Then, the electric field generated by the region 2 field-aligned current would have dominated over the convection electric field driven by the solar wind and the IMF.

[14] Event 2, on the other hand, cannot be simply attributed to the northward turning of the IMF because the IMF remained southward throughout the event. Provisional *AL* index indicates that the substorm expansion phase commenced at 0615 UT, followed by a recovery phase at 0629 UT. This implies a delay of 12 min between the commencement of the substorm expansion and the emergence of event 2. The overshielding event associated with a substorm was also studied by *Kikuchi et al.* [2000b], who speculated that the shielding electric field overcame the convection electric field following the abrupt weakening of the convection electric field during the substorm. The physical mechanism responsible for the abrupt weakening of the convection electric field during the substorm is unclear. One possibility is shrinkage of the polar cap. Observations have indicated that shrinkage of the polar cap occurs with a delay of 20–50 min following substorm expansion phase onset [e.g., *Taylor et al.*, 1996]. Weakening of the convection electric field in the subauroral region may thus have occurred because of shrinkage of the polar cap without a decrease in the cross–polar cap potential drop. However, no direct evidence has been adduced that the

shrinkage of the polar cap results in the shielding/overshielding condition.

[15] It is also possible, however, that a magnetospheric current excluded from the simulation is responsible for the overshielding condition of event 2. For example, it is possible that a sudden earthward displacement of hot magnetospheric ions from the nightside plasma sheet could have occurred immediately following enhancement of the convection electric potential. The newly injected ions would have enhanced the plasma pressure in the evening-midnight sector (see Figure 4), and produced an inertial current flowing westward near the earthward portion of the newly injection ions. Part of the inertial current would have been converted to a field-aligned current flowing into the ionosphere near the westernmost portion of the inertial current to conserve electric current. This converted field-aligned current could then have resulted in enhancement of the shielding electric field. Such a mechanism is consistent with the timing of event 2, which took place just after the sudden change in IMF B_z from -5 nT to -10 nT. This model also predicts the shielding/overshielding condition around 0540 UT at which the IMF turns southward. However, there is no clear evidence that the shielding/overshielding condition occurred at the same time in the radar data. A self-consistent simulation including the inertial current and a detailed statistical study is considered necessary in order to investigate this mechanism in greater depth.

5. Conclusion

[16] The SuperDARN Hokkaido radar observed at least two subauroral negative Doppler velocity events in the afternoon sector during an intense magnetic storm on 15 December 2006. The mean velocity of the flow was -46 m/s, reaching a maximum speed of approximately 80 m/s. The flow was directed antisunward, opposite to the normal direction observed in the corresponding region. Event 1 (0519–0533 UT) occurred immediately after the northward turning of the IMF, and is attributable to an overshielding condition caused by an abrupt decrease in the convection electric potential. Simulations of the line-of-sight velocity along a radar beam assuming such a mechanism are consistent with these observations. Event 2 (0627–0637 UT) occurred during a southward oriented IMF and is likely attributable to abrupt contraction of the polar cap or strengthening of the inertial current near the inner edge of newly injected ions from the nightside plasma sheet. However, neither fully accounts for the observations.

[17] **Acknowledgments.** IMF and solar wind data were provided by Norman F. Ness (ACE/MFI) and David J. McComas (ACE/SWEPAM). The authors thank Daniel R. Weimer for source code of the empirical convection electric field model and Nikolai A. Tsyganenko for the empirical magnetic field model. Geotail/MGF data were provided by Tsugunobu Nagai. The DMSP particle detectors were designed by Dave Hardy of AFRL, and data were obtained from JHU/APL. We thank Dave Hardy, Fred Rich, and Patrick Newell for their use. Provisional *Dst* and auroral electrojet (*AE*) indices were provided by the World Data Center for Geomagnetism, Kyoto. Ryuho Kataoka is also gratefully acknowledged for valuable discussions. Grateful acknowledgment is due to Robert W. Spiro and Stanislav Y. Sazykin for supporting calculation of ionospheric conductivities and electrostatic potential. This study was supported by the Program for Improvement of Research Environment for Young Researchers from the Special Coordination Funds for Promoting Science and Technology (SCF) commissioned by the Ministry of Education, Culture, Sports, Science and Technology (MEXT) of Japan.

[18] Wolfgang Baumjohann thanks the reviewers for their assistance in evaluating the paper.

References

Bilitza, D. (1997), International Reference Ionosphere—Status, 1995/96, *Adv. Space Res.*, *20*, 1751.

Bristow, W. A., and R. A. Greenwald (1997), On the spectrum of thermospheric gravity waves observed by the Super Dual Auroral Radar Network, *J. Geophys. Res.*, *102*(A6), 11,585.

Chakrabarty, D., R. Sekar, R. Narayanan, A. K. Patra, and C. V. Devasia (2006), Effects of interplanetary electric field on the development of an equatorial spread *F* event, *J. Geophys. Res.*, *111*, A12316, doi:10.1029/2006JA011884.

Ebihara, Y., M.-C. Fok, R. A. Wolf, T. J. Immel, and T. E. Moore (2004), Influence of ionosphere conductivity on the ring current, *J. Geophys. Res.*, *109*, A08205, doi:10.1029/2003JA010351.

Fejer, B. G., C. A. Gonzales, D. T. Farley, and M. C. Kelley (1979), Equatorial electric fields during magnetically disturbed conditions: 1. The effect of the interplanetary magnetic field, *J. Geophys. Res.*, *84*, 5797.

Fejer, B. G., R. W. Spiro, R. A. Wolf, and J. C. Foster (1990), Latitudinal variation of perturbation electric fields during magnetically disturbed periods: 1986 SUNDIAL observations and model results, *Ann. Geophys.*, *8*, 441.

Fok, M.-C., R. A. Wolf, R. W. Spiro, and T. E. Moore (2001), Comprehensive computational model of Earth's ring current, *J. Geophys. Res.*, *106*, 8417.

Foster, J. C., and H. B. Vo (2002), Average characteristics and activity dependence of the subauroral polarization stream, *J. Geophys. Res.*, *107*(A12), 1475, doi:10.1029/2002JA009409.

Goldstein, J., R. W. Spiro, P. H. Reiff, R. A. Wolf, B. R. Sandel, J. W. Freeman, and R. L. Lambour (2002), IMF-driven overshielding electric field and the origin of the plasmaspheric shoulder of May 24, 2000, *Geophys. Res. Lett.*, *29*(16), 1819, doi:10.1029/2001GL014534.

Gonzales, C. A., M. C. Kelley, B. G. Fejer, J. F. Vickrey, and R. F. Woodman (1979), Equatorial electric fields during magnetically disturbed conditions: 2. Implications of simultaneous auroral and equatorial measurements, *J. Geophys. Res.*, *84*, 5803.

Greenwald, R. A., et al. (1995), DARN/SuperDARN: A global view of high-latitude convection, *Space Sci. Rev.*, *71*, 763.

Greenwald, R. A., K. Oksavik, P. J. Erickson, F. D. Lind, J. M. Ruohoniemi, J. B. H. Baker, and J. W. Gjerloev (2006), Identification of the temperature gradient instability as the source of decameter-scale ionospheric irregularities on plasmapause field lines, *Geophys. Res. Lett.*, *33*, L18105, doi:10.1029/2006GL026581.

Hardy, D. A., M. S. Gussenhoven, R. Raistrick, and W. J. McNeil (1987), Statistical and functional representations of the pattern of auroral energy flux, number flux, and conductivity, *J. Geophys. Res.*, *92*, 12,275.

Hedin, A. E. (1991), Extension of the MSIS thermospheric model into the middle and lower atmosphere, *J. Geophys. Res.*, *96*, 1159.

Hosokawa, K., T. Iyemori, A. S. Yukimatu, and N. Sato (2001), Source of field-aligned irregularities in the subauroral *F* region as observed by the SuperDARN radars, *J. Geophys. Res.*, *106*, 24,713.

Hudson, M. K., and M. C. Kelley (1976), The temperature gradient instability at the equatorward edge of the ionospheric plasma trough, *J. Geophys. Res.*, *81*, 3913.

Jaggi, R. K., and R. A. Wolf (1973), Self-consistent calculation of the motion of a sheet of ions in the magnetosphere, *J. Geophys. Res.*, *78*, 2852.

Kelley, M. C., B. G. Fejer, and C. A. Gonzales (1979), An explanation for anomalous equatorial ionospheric electric fields associated with a northward turning of the interplanetary magnetic field, *Geophys. Res. Lett.*, *6*, 301.

Kikuchi, T., M. Pinnock, A. Rodger, H. Lühr, T. Kitamura, H. Tachihara, M. Watanabe, N. Sato, and M. Ruohoniemi (2000a), Global evolution of a substorm-associated DP 2 current system observed by SuperDARN and magnetometers, *Adv. Space Res.*, *26*, 121.

Kikuchi, T., H. Lühr, K. Schlegel, H. Tachihara, M. Shinohara, and T.-I. Kitamura (2000b), Penetration of auroral electric fields to the equator during a substorm, *J. Geophys. Res.*, *105*, 23,251.

Kikuchi, T., K. K. Hashimoto, T.-I. Kitamura, H. Tachihara, and B. Fejer (2003), Equatorial counterelectrojets during substorms, *J. Geophys. Res.*, *108*(A11), 1406, doi:10.1029/2003JA009915.

Nishida, A., N. Iwasaki, and T. Nagata (1966), The origin of fluctuations in the equatorial electrojet: A new type of geomagnetic variation, *Ann. Geophys.*, *22*, 478.

Nishitani, N., and T. Ogawa (2005), Model calculations of possible ionospheric backscatter echo area for a mid-latitude HF radar, *Adv. Polar Upper Atmos. Res.*, *19*, 55.

Ossakow, S. L., and P. K. Chaturvedi (1979), Current convective instability in the diffuse aurora, *Geophys. Res. Lett.*, *6*, 332.

Peymirat, C., A. D. Richmond, and A. T. Kobea (2000), Electrodynamic coupling of high and low latitudes: Simulations of shielding/overshielding effects, *J. Geophys. Res.*, *105*, 22,991.

Ruohoniemi, J. M., and R. A. Greenwald (2005), Dependencies of high-latitude plasma convection: Consideration of interplanetary magnetic field, seasonal, and universal time factors in statistical patterns, *J. Geophys. Res.*, *110*, A09204, doi:10.1029/2004JA010815.

Samson, J. C., R. A. Greenwald, J. M. Ruohoniemi, and K. B. Baker (1989), High-frequency radar observations of atmospheric gravity waves in the high-latitude ionosphere, *Geophys. Res. Lett.*, *16*, 875.

Senior, C., and M. Blanc (1984), On the control of magnetospheric convection by the spatial distribution of ionospheric conductivities, *J. Geophys. Res.*, *89*, 261.

Southwood, D. J. (1977), The role of hot plasma in magnetosphere convection, *J. Geophys. Res.*, *82*, 5512.

Spiro, R. W., and R. A. Wolf (1984), Electrodynamics of convection in the inner magnetosphere, in *Magnetospheric Currents*, *Geophys. Monogr. Ser.*, vol. 28, edited by T. A. Potemra, p. 248, AGU, Washington, D. C.

Spiro, R. W., R. A. Wolf, and B. G. Fejer (1988), Penetration of high-latitude-electric-field effects to low latitudes during SUNDIAL 1984, *Ann. Geophys.*, *6*, 39.

Taylor, J. R., T. K. Yeoman, M. Lester, B. A. Emery, and D. J. Knipp (1996), Variations in the polar cap area during intervals of substorm activity on 20–21 March 1990 deduced from AMIE convection maps, *Ann. Geophys.*, *14*, 879.

Toffoletto, F., S. Sazykin, R. Spiro, and R. Wolf (2003), Inner magnetospheric modeling with the Rice convection model, *Space Sci. Rev.*, *107*, 175.

Tsyganenko, N. A. (1995), Modeling the Earth's magnetospheric magnetic field confined within a realistic magnetopause, *J. Geophys. Res.*, *100*, 5599.

Tsyganenko, N. A., and D. P. Stern (1996), A new-generation global magnetosphere field model, based on spacecraft magnetometer data, *ISTP Newsl.*, *6*(1), 21.

Vasyliunas, V. M. (1970), Mathematical models of magnetospheric convection and its coupling to the ionosphere, in *Particles and Fields in the Magnetosphere*, edited by M. McCormac, p. 60, D. Reidel, Norwell, Mass.

Weimer, D. R. (2001), An improved model of ionospheric electric potentials including substorm perturbations and application to the Geospace Environment Modeling November 24, 1996, event, *J. Geophys. Res.*, *106*, 407.

Weimer, D. R. (2005), Improved ionospheric electrodynamic models and application to calculating Joule heating rates, *J. Geophys. Res.*, *110*, A05306, doi:10.1029/2004JA010884.

Wolf, R. A. (1970), Effects of ionospheric conductivity on convection flow of plasma in the magnetosphere, *J. Geophys. Res.*, *75*, 4677.

Y. Ebihara, Institute for Advanced Research, Nagoya University, Furocho, Chikusa-ku, Nagoya 464-8601, Japan. (ebihara@stelab.nagoya-u.ac.jp)

M.-C. Fok, NASA GSFC, Code 673, Greenbelt, MD 20771, USA. (mei-ching.fok@gsfc.nasa.gov)

K. Hosokawa, Department of Information and Communication Engineering, University of Electro-Communications, 1-5-1, Chofugaoka, Chofu, Tokyo 182-8585, Japan. (hosokawa@ice.uec.ac.jp)

T. Kikuchi and N. Nishitani, Solar-Terrestrial Environment Laboratory, Nagoya University, Furo-cho, Chikusa-ku, Nagoya 464-8601, Japan. (kikuchi@stelab.nagoya-u.ac.jb; nisitani@stelab.nagoya-u.ac.jp)

T. Ogawa, Solar-Terrestrial Environment Laboratory, Nagoya University, 3-13 Honohara, Toyokawa, Aichi 442-8507, Japan. (ogawa@stelab.nagoya-u.ac.jp)